Iran. J. Radiat. Res., 2011; 9(1): 15-28

Monte Carlo estimation of electron contamination in a 18 MV clinical photon beam

M. Allahverdi[1], M. Zabihzadeh[2], M.R. Ay[1,3*], S.R. Mahdavi[4], M. Shahriari[5], A. Mesbahi[6], H. Alijanzadeh[7]

[1]Department of Medical Physics and Biomedical Engineering, Tehran University of Medical Sciences, Tehran, Iran
[2]Department of Medical Physics, Jondishapour University of Medical Sciences, Ahvaz, Iran
[3]Research Center for Science and Technology in Medicine, Tehran University of Medical Sciences, Tehran, Iran
[4]Department of Medical Physics, Iran University of Medical Sciences, Tehran, Iran
[5]Department of Nuclear Engineering, Shahid Beheshti University, Tehran, Iran
[6]Department of Medical Physics, Tabriz University of Medical Sciences, Tabriz, Iran
[7]Department of Physics, Science faculty, Mazandaran University, Babolsar, Iran

Background: The electron contamination may reduce or even diminish the skin sparing property of the megavoltage beam. The detailed characteristics of contaminant electrons are presented for different field sizes and cases. ***Materials and Methods:*** The Monte Carlo code, MCNPX, has been used to simulate 18 MV photon beam from a Varian Linac-2300 accelerator. All dose measurements were carried out using a PTW-MP2 scanner with an ionization chamber (0.6 CC) at the water phantom. ***Results:*** The maximum electron contaminant dose at the surface ranged from 6.1 % for 5 × 5 cm^2 to 38.8 % for 40 × 40 cm^2 and at the depth of maximum dose was 0.9 % up to 5.77 % for the 5 × 5 cm^2 to the 40 × 40 cm^2 field sizes, respectively. The additional contaminant electron dose at the surface for the field with tray increased 2.3 % for 10 × 10 cm^2, 7.3 % for 20 × 20 cm^2, and 21.4 % for 40 × 40 cm^2 field size comparing to the standard field without any accessories. This increase for field with tray and shaping block was 5.3 % and 13.3 % for 10 × 10 and 20 × 20 cm^2, respectively, while, the electron contamination decreased for the fields with wedge, i.e. 2.2 % for the 10 × 10 cm^2 field. ***Conclusion:*** The results have provided more comprehensive knowledge of the high-energy clinical beams and may be useful to develop the accurate treatment planning systems capable of taking the electron contamination in to account. **Iran. J. Radiat. Res., 2011; 9(1): 15-28**

Keywords: *Monte Carlo simulation, MV photon beam, electron contamination, relative absorbed dose.*

INTRODUCTION

Contamination of therapeutic photon beam with the charged particles shift the depth of maximum dose toward the shallower depths increases the surface dose, and deteriorates the skin sparing as an advantage with high energy photon therapy. These contaminating charged particles (electrons and positrons) are produced by photon interactions in the Linac head components, the air volume between head, and phantom surface. Furthermore, different accessories located in the beam path could increase or decrease the effects on the surface doses depending on their material and distance to the isocenter. It was found that contaminating electrons shifted the depth of maximum dose toward the shallower depths with field size in high energy photon beams [(1)]. Some authors reported that the flattening filter and the beam monitor chamber are the main sources of electron contamination [(2, 3)]. Furthermore, the air volume was also reported as a major source at extended SSDs [(4)]. It was suggested that reducing the field size lead to scattering out of the contaminating electrons and thus to reduce the surface dose [(5-7)].

Several studies used a magnetic field to remove the contaminating electrons

Corresponding author:
Dr. Mohammad Reza Ay,
Department of Medical Physics and Biomedical Engineering, Tehran University of Medical Sciences, Tehran, Iran.
Fax: *+98 21 64053255*
E-mail: *mohammadreza_ay@tums.ac.ir*

originated from the Linac's head [8-10]. Some authors reported that replacing air volume between collimators and surface by a helium bag could remove the air produced electrons [11]. A lead filter has been reported as the most efficient material among the high-Z filters to spread out the contaminating electrons and preventing them to reach the surface [12]. The presence of modifiers in the beam trajectory can modify the beam quality and cause some changes in the dosimetry parameters, especially in build up rejoin [13-15].

Using convolution-based, three-dimensional dose calculation models in treatment planning systems (TPS) is popular to calculate energy deposition. It worth's to emphasize that the photon kernels implemented in the TPS do not consider the contribution of electron contamination in the build-up region and use pre-calculated energy deposition kernels for photon-only beams. However, some TPSs which consider these contaminations assume that electron contamination does not vary with SSD or added accessories [16, 17]. Furthermore, these contaminant electrons have an important effect on beam quality specification as reported by AAPM (*American Association of Physicists in Medicine)* in TG-51 protocol [4, 18]. This study aims to provide more comprehensive information on the contaminating electrons associated with therapeutic photon beams for different field sizes, SSDs and accessories. Separation of the contaminant electron dose for each clinical situation in build up depths and adding them to photon dose in TPSs improve the accuracy of determination of dose deposition.

MATERIALS AND METHODS

Experimental measurement

All dose measurements including depth dose curves and dose profiles were carried out using a PTW-MP2 scanner with an ionization chamber at the water phantom ($50 \times 50 \times 50$ cm^3). The cylindrical chamber had an inner diameter of 6 mm and the effective point of measurement was taken to be 0.6 r_{inner} (where r_{inner} is the radius of the chamber cavity) upstream of the centre of the chamber, consistent with the AAPM TG-51 protocol [18]. The scanning system had a position accuracy of ≤ 1 mm and a reproducibility of ≤ 0.1 mm.

Monte Carlo calculation

MCNPX version 2.4.0 Monte Carlo code was used to model photon beams from the Varian 2300C/D linac, 18 MV [19]. MCNPX is a well known general purpose Monte Carlo code developed at Los Alamos National Laboratories. It extends the transport capability of Monte Carlo program to include 34 particles over a more complete energy range. This range (<150 MeV) of energy can be used to simulate radiation transport of these particles in radiation therapy applications. Figure 1 shows the set up of the simulated geometry for the Varian 2300C/D linac.

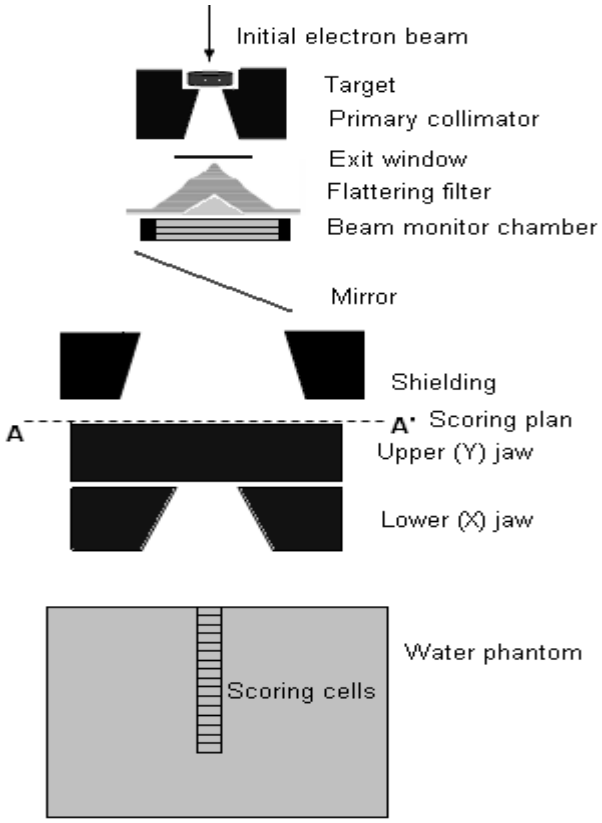

Figure 1. Schematic drawing of Varian treatment head and water phantom.

The simulated model included the bremsstrahlung target, the primary collimator, the vacuum window, the flattening filter, the monitor ion chamber, the mirror, and the upper and lower jaws. Beam monitoring chamber and flattening filter were accurately modeled due to the fact that they are the main sources of contaminating electrons. This detailed description of the geometry required for the accurate simulation was provided by the manufacturer. The electron and photon cut off energies were set to 0.5 MeV and 0.01 MeV, respectively. No photon interaction forcing and no Rayleigh scattering were used.

The exact energy and radial spread of the hitting electrons to the target were unknown and must be obtained by calibrating each spectral distribution against the corresponding depth dose curve and profiles. Adjusting the calculated depth dose curves and profiles with the measurements is time consuming, but must be done well due to its important role in obtaining the best match between Monte Carlo calculated and measured dose for a given beam energy. It should be noted that the central axis-depth dose curves are dependent to the hitting electron energy while the dose profiles (especially for larger field sizes) are more affected by the radial spread of these electrons. In the present study the range of the primary mean electron energy was ranged from 17.7 to 18.4 MeV. The final incident electrons had a Gaussian energy distribution with a full width at half maximum (FWHM) of 1 MeV and centered at 18.2 MeV for the 18 MV photon beam. The electron beam radial intensity distribution was also set to be a Gaussian with the FWHM of 1.4 mm.

The F2 and *F2 tallies were used to calculate corresponding parameters at the downstream surface of target and fattening filter. The F4 and *F4 tallies were used to calculate the fluence profiles, the energy spectra, and the mean energy profiles at the phantom surface. The dose distribution from photons (including secondary electrons and electron contamination) was calculated, using the *F6 tally (in units of MeV/g) for electrons (*F6:E) since photons' transfered all their energy to electrons in photoatomic interactions. The F6:E tally is a new feature of MCNPX that is not installed in pervious versions such as MCNP-4C. The F6 tally for charged particles is a track-length estimator based on the use of the restricted or total stopping power of the particle [19].

The maximum statistical uncertainty of our results at the depth of maximum dose for different field sizes and for several cases was about 2 %. For depth dose calculations in water phantom, a cylinder with a radius of one-tenth the size of the open field size was defined and divided into scoring cells with 2 mm height along the beam central axis. For beam profile calculations the primary cylinder was located at the considered depth vertically to the beam central axis with the radius of 2 mm; therefore, the dose resolution was 2 mm in this study.

A surface scoring plane (AA' at figure 1) was defined at the upstream surface of upper secondary collimator and scored all photons and electrons which crossed it. A total of 1×10^8 electron histories were simulated. The size of a phase space file was about 4 GB. The CPU used for the simulation was a Pentium IV with 2.5 GHz processors. By reading the data from this surface source the researchers calculated the energy spectra, the mean energy profiles, and fluence profiles at the surface of phantom. The air generated-electron (between the secondary collimator and the phantom surface) for these parameters could also be obtained by inserting a 0.001cm-thick cell with zero importance for electrons (IMP: E 0) at downstream surface of lower secondary collimator to remove the head- generated electrons. The corresponding data of head-generated electrons was extracted by subtracting the total electrons with the air-generated electrons.

Defining a 0.001cm-thick rectangular cell (50×50 cm^2) with zero importance for electrons (IMP: E 0, IMP: P 1) on the phan-

tom surface obtained the depth dose curves and the dose profiles from photon beam only (free-electron contaminant, clean beam). Subtracting the dose curve and profile from standard field (include total contamination) with those from the clean field resulted the electron contaminant contribution. The mean energy of energy spectra were calculated by the formula

$$\bar{E} = \frac{\sum_{0}^{E_{max}} \phi_E \, E dE}{\sum_{0}^{E_{max}} \phi_E \, dE} \qquad (1)$$

Where $\bar{E}$ is the mean energy, ϕ_E is the photon fluence at energy bin (dE), and E_{max} is the maximum energy of photon.

All measured absorbed dose curves were normalized at the depth of maximum dose on the central axis. The Monte Carlo calculated absorbed dose curve was scaled at a depth of 10 cm, so that it had the same value as that of the corresponding measured data. This depth was chosen, because no electrons could reach it in water phantom at energies below 18 MV. The first calculation point in the depth dose curves was at a depth of 1 mm as center of the first scoring cell of phantom on the beam central axis. Hence, the y-axis has been set to cross the x-axis at this depth in the figures. An average value of the two calculated points on both sides of the normalization depth was taken in order to reach exact depth of 10 cm and minimize the influence from statistical fluctuations.

Analytical method

Beauvais *et al.* (1993) proposed an analytical method to obtain contaminant electron doses [20]. Their model, using a linear apparent attenuation coefficient, is described by the following equation,

$$D_c(d) = A. \exp(-\gamma. d) \qquad (2)$$

Where D_c is the electron contaminant dose, d is the depth inside the phantom in mm, A is the surface dose, and γ is the rate of dose attenuation with depth in mm^{-1}. This model (equation 2) has been used by other authors as well [10, 21, 22]. Zhu and Palta (1998) reported a new model that was a refinement of a pure exponential function and declared that fits the measured data much better [9]. Nevertheless, the model from Beauvais *et al.* (1993) have been used for comparing with our data while the values of A and γ for 18 MV have been extracted from the study reported by Zhu and Palta (1998) [9, 20].

RESULTS

MC-calculated PDD (percentage depth dose) curves and beam profiles were compared with the measurements to validate our MC model. There was good agreement between the measurements and calculations for beam profiles and PDD curves (figures 5 and 8). For beam profiles, maximum local differences less than 2%, were seen for flat regions, but it increased to 13% for regions located out of field for the deepest considered depth of 20 cm (figure 5). Local differences of less than 1 % were seen for PDD values in descending part up to 30-cm depth between measurement and calculation, but it increased up to 12% for buildup regions (figure 8). The statistical uncertainty of the simulations (one σ interval) was below 1 % for the depth-dose profiles. The 40 × 40 cm^2 field size resulted in a statistical uncertainty of down to 4.6 %.

Photon and contaminant electron fluence spectra

Figures 2a and b present spectra of photons and contaminating electrons (number of photons or electrons per MeV per incident electron on the target) at the phantom surface for the 10 × 10 cm^2 and 40 × 40 cm^2 fields respectively. Only the particles which were inside the defined field at the phantom surface were counted. The average energy of reached photons to the phantom surface was 4.72 MeV and 3.63 MeV for the 10 × 10 cm^2 and 40 × 40 cm^2

fields, respectively; while it was 3.65 MeV and 3.25 MeV for electrons. The average photon energy inside the field was less than 1/3 of the nominal beam energy. The total count per MeV per incident electron on the target for contaminant electrons was 0.13% and 0.43% magnitude lower than that of photons for the 10 × 10 cm² and 40 × 40 cm² fields, respectively. The initial sudden fall off in the fluence of low-energy electrons was due to the cut off energy of 0.5 MeV for the transport of electrons in order to run time saving.

Mean energy distributions

The mean energy of photons was relatively flat inside the 10 × 10 cm² field (4.62 MeV on the central axis) and shows a sharp fall off at the edge of the field (2.96 MeV) as shown in figure 3a. The mean energy of photons for the 40 × 40 cm² field (as shown in figure 3b) decreased gradually inside the field (from 4.49 MeV on the central axis to 2.85 MeV at the field border) and showed a rapid drop at the field edge (1.99 MeV) then decreased gradually at the off-axis distances. While the mean energy distribution of contaminant electrons showed a slow decrease for 10 × 10 cm² field away from central axis, it remained approximately unchanged inside the 40 × 40 cm² field and then decreased at the off-axis distances from the field edge. As can be seen, except for the initial off-axis distance in the case of the 40 × 40 cm² field, the mean energy of contaminant electrons was higher than that of photons.

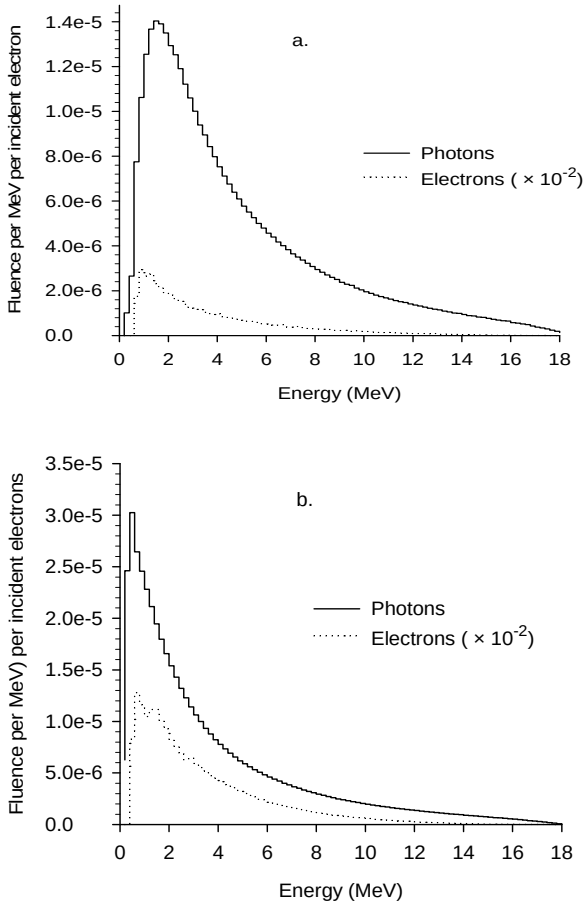

Figure 2. The fluence spectra of photons and electrons at the phantom surface (defined at SSD = 100 cm) inside a. the 10 × 10 cm² and b. the 40 × 40 cm² field sizes.

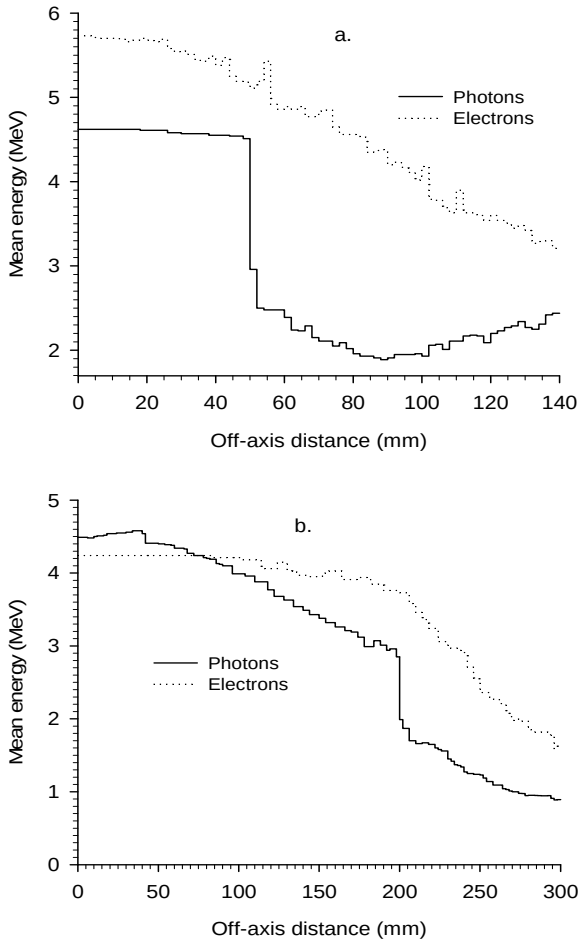

Figure 3. The mean energies of photons and electrons at the phantom surface as a function of off-axis distance for a. 10 × 10 cm² and b. 40 × 40 cm² field size at SSD = 100 cm.

Photon and electron fluence profiles

Figures 4a and b show the fluence profiles of photons and electrons at the phantom surface (SSD = 100 cm) for the 10 × 10 cm² and 40 × 40 cm² fields respectively. For the 10 × 10 cm² field, the photon's fluence was relatively constant (an increase up to 8.5 %) until a sharp decrease at the field edge. For a 40 × 40 cm² field, the photon's fluence profile increased up to 26.8 % away from central axis. There was no sharp decrease outside the field for contaminant electron fluence. The accelerator head generated electrons had the majority contribution of contaminant electrons, 80.2 % for field size of 10 × 10 cm² and 80.7 % for field size of 40 × 40 cm².

Relative absorbed dose profiles

Figure 5 shows the comparisons between measured and the Monte Carlo calculated dose profiles at various depths for the 40 × 40 cm² field. The calculated dose profiles were in good agreement with the measured values. Maximum local differences, less than 2%, were seen for flat region, but it increased to 13% for region located out of field for deepest considered depth of 20 cm. The Monte Carlo calculated surface dose profiles across 10×10 cm² and 40×40 cm² fields are shown in figures 6a and b, respectively. The surface dose was the average dose in each voxel referred to depth of 1 mm. These data indicated that the contaminant electron dose has maximum value in central axis, and it gradually decreased at the off-axis distances while the photon dose showed an increase toward the field border and then followed by a sharp fall off. This was expected, as earlier discussed in parts 3.2 and 3.3. It is also seen that the contaminant electrons has the majority contribution of the surface dose outside from the field edge.

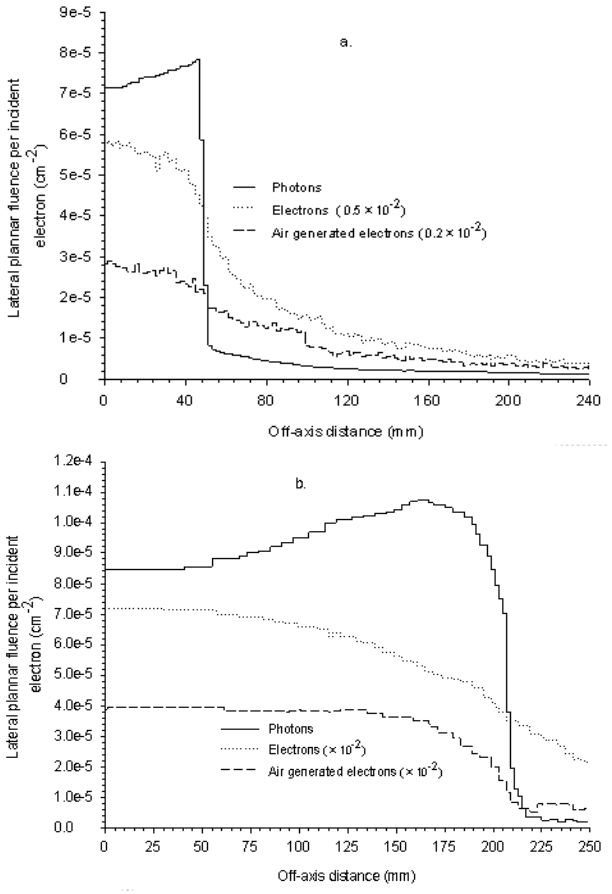

Figure 4. The planar fluence profiles of photons and electrons at the phantom surface for a. 10 × 10 and b. 40 × 40 cm² field size at SSD =100 cm.

Relative absorbed dose only from photon beam

The PDD curves of clean photon beam for different fields at SSD = 100 cm were depicted in figure 7. Curves were normalized to the value at the maximum depth dose. As it can be seen, no significant variations were discernible for different field sizes, before reaching the electronic equilibrium. These curves had good

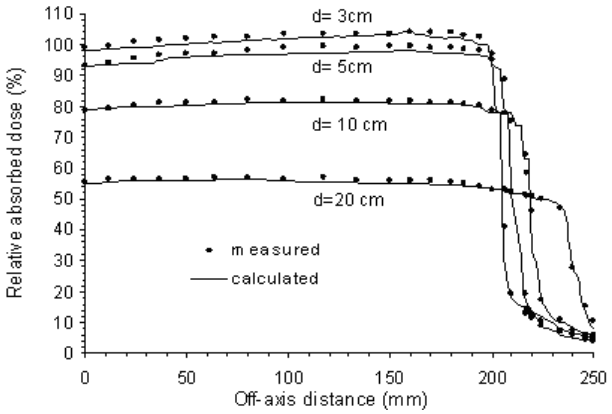

Figure 5. Comparison of the Monte Carlo dose profile calculations versus water phantom measurements for the 40 × 40 cm² field size at depths of 3, 5, 10 and 20 cm from up to down, respectively.

agreement on depth of maximum dose (better than 2 %) that indicated these calculated curves to be free of electron contaminations.

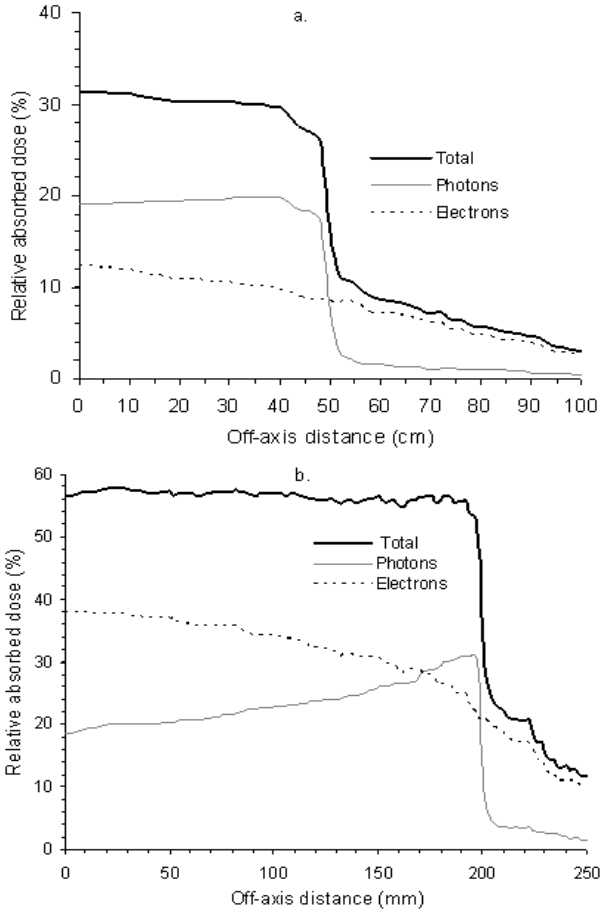

Figure 6. Monte Carlo calculated dose profiles from incident photons and contaminant electrons across the a. 10 × 10 cm² and b. 40 × 40 cm² fields defined at SSD=100 cm. The surface dose is the average dose in each voxel referred to depth of 1 mm.

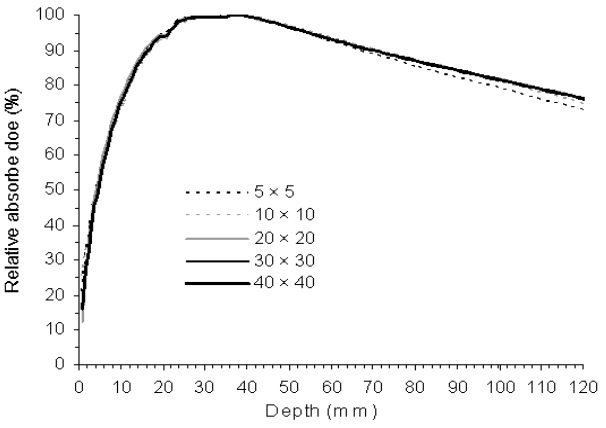

Figure 7. Comparison of depth dose curves in pure photon beam from clean fields normalized at depth of maximum dose at SSD=100 cm.

Standard field without any accessories

Depth dose curves for 10 × 10 cm² and 40 × 40 cm² field sizes at SSD = 100 cm are shown in figures 8a and b, respectively. As shown, the electron contribution from Linac head to the electron contamination was greater compared to the electron contribution from air. As it is seen in figure 8b, the dose from contaminant electrons is even higher than the dose from the incident photons for the 40 × 40 cm² field size. For a 10 × 10 cm² field size the contribution from the Linac head to the electron contamination dose was 3 times lager than the contribution from the air at SSD = 100 cm.

Figure 9 shows the field size dependence of the electron contamination. These curves were obtained with subtracting standard curves from the clean curves. The maximum uncertainties for the absorbed dose curves of standard and clean fields were higher than 2% and 1%; respectively. As shown in figure 9, the maximum electron contaminant dose at the surface ranged from 6.1 % for 5 × 5 cm² to 38.8 % for 40 × 40 cm². The electron contamination dose at depth of maximum dose was 0.9 %, 2.33 %, 4.13 %, 4.65 % and 5.77 % for the field sizes of 5 × 5 cm², 10 × 10 cm², 20 × 20 cm², 30 × 30 cm², 40 × 40 cm², respectively. Figure 9 also included the curves from the analytical method proposed by Beauvais *et al.* [20]. As can be seen, the analytically obtained curves have been in rather good agreement with the calculated curves, except in the surface region. Figure 10 shows SSD dependence for relative surface dose of contaminant electrons for 40 × 40 cm² field size. The doses had maximum values at SSD = 90 cm for each depths. The discrepancies of doses for different depths ranged at calculation uncertainties for SSD of 100, 110, and 120 cm (except at depth of 5 mm for SSD = 120 cm). Decrease of the electron contaminant dose was pronounced for shallower depths (5 and 11 mm) at SSD = 140 cm.

Field with shadow tray accessory

The relative absorbed dose from fields

with attenuating tray is depicted in figure 11. The contaminant electron dose increased when the tray insert in place compared to standard field without tray accessory.

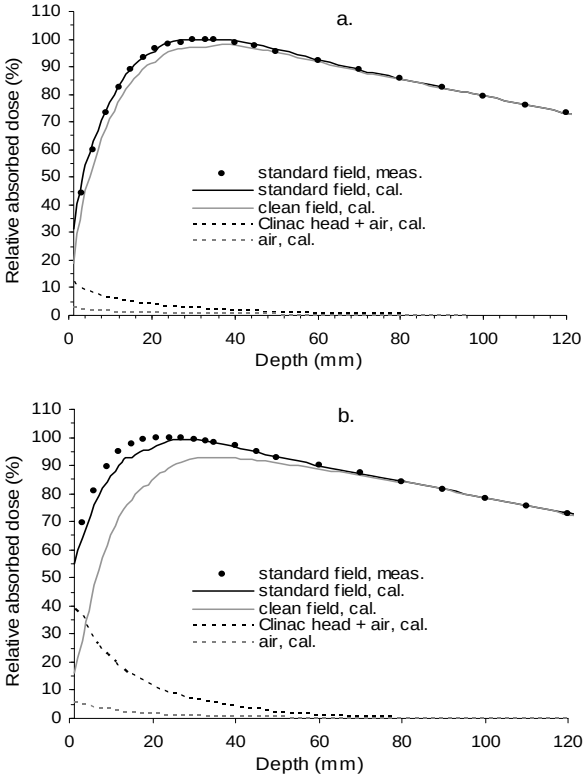

Figure 8. Depth dose curves calculated at SSD = 100 cm with the field sizes of a. 10 × 10 cm² and b. 40 × 40 cm² . The points are measured data for standard field (meas.) and the lines are Monte Carlo calculated data (cal.). The black line represents a standard curve, the gray line represents a clean curve, the black dashed line represents the electron contamination from Linac head and air, and the gray dashed line represents the electron contamination only from air column between head and phantom.

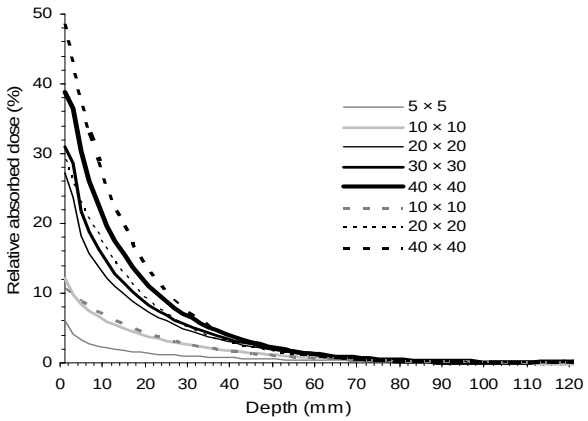

Figure 9. comparison of contaminant electron dose at different field sizes at SSD= 100 cm. The solid lines are calculated curves and the dashed lines are fitting curves according to proposed function by Beauvais *et al.* (1993) [20].

Increasing the field size increased the magnitude of this increase. The additional contaminant electron dose at the surface increased 2.3 % for 10 × 10 cm², 7.3 % for 20 × 20 cm², and 21.4 % for 40 × 40 cm² field size compared to the fields without tray.

Field with a block on tray

As shown in figure 12, adding a square block on tray increased the contaminating electrons dose. The dotted lines in figure 12 are the exponential fitting curves of our data. This increase compared to the field without any accessory was 5.3 % and 13.3 % for 10 × 10 and 20 × 20 cm², respectively. On the other hand, Comparing the maximum contaminating electron dose at the surface for the field with block on tray and field

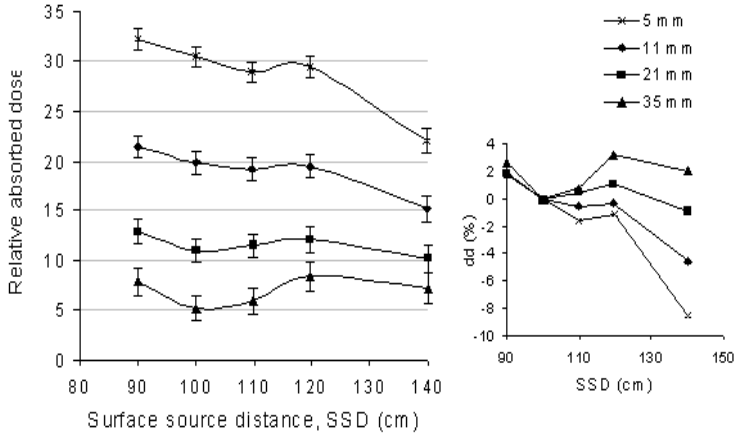

Figure 10. The SSD dependence of relative absorbed dose from contaminant electrons at different depths of buildup region for 40 × 40 cm² field size. The right insert is the additional amount of relative absorbed dose for different SSDs compare to the SSD=100 at the each depths.

with only tray showed that the dose increase 3.5 % for 10 × 10 cm² and 4.4 % for 20 × 20 cm² when the block was added on tray.

Field with wedge

The comparison of electron contamination depth dose for wedged field is shown in figure 13. Inserting a steel wedge into the beam decreased the relative absorbed dose comparing to other studied cases. The dotted lines in figure 13 are the exponential fitting curves according to our data. For example the magnitude decreased for the field sizes of 10 × 10 and 20 × 20 cm² was 2.2%, 0.5% and 8.0%, 13.9% compared to the fields without any accessory and fields with tray and shaping block, respectively.

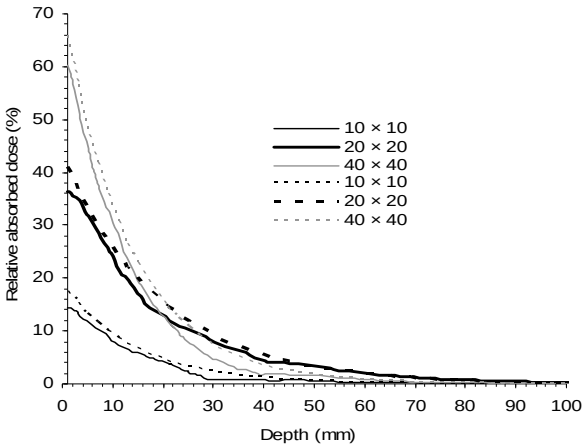

Figure 11. Relative absorbed dose from contaminant electrons of fields aluminum tray (0.6 cm thick) at SSD=100 cm for field sizes of 10 × 10, 20 × 20, and 40 × 40 cm². The solid lines are calculated curves and the doted lines are analytical fitted curves.

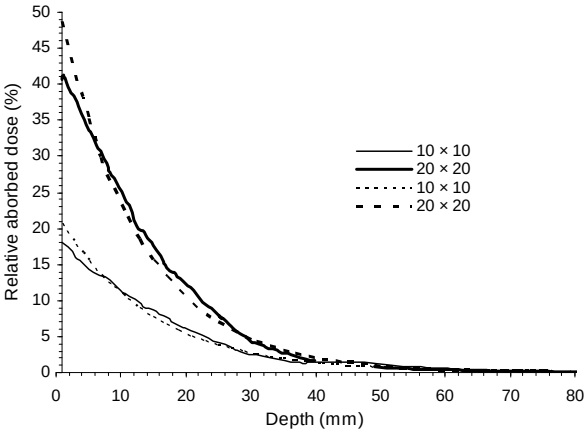

Figure 12. Relative absorbed dose from contaminant electrons of fields with tray and shaping block at SSD=100 cm for field sizes of 10 × 10 and 20 × 20 cm². The solid lines are calculated curves and doted lines are analytical fitted curves (on our data).

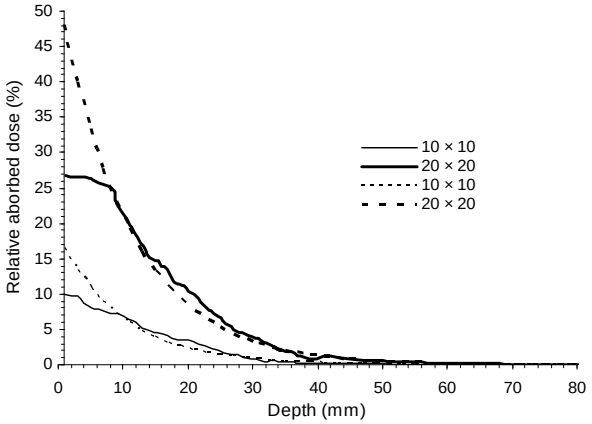

Figure 13. Relative absorbed dose from contaminant electrons of fields with wedge at SSD = 100 cm for field sizes of 10 × 10 and 20 × 20 cm². The solid lines are calculated curves and doted lines are analytical fitted curves (on our data).

DISCUSSION

Fluence spectra of photons peak at 1.30 MeV and 0.50 MeV for the 10 × 10 cm² and 40 × 40 cm² fields which are consistent with ones reported by Ding (2002 b) [23] (1.5 MeV and 0.5 MeV for the 10 × 10 cm² and 40 × 40 cm² fields respectively). Following by the sharp drop, a slight decrease occurred and then a slight increase was resulted for the mean energy of photons at the larger off-axis distances (figure 3a). The increase was due to hardening effect of collimators, since the transferred photons through the 7 cm thick tungsten collimators had much higher energies. On the central axis (figure 4a, b), the contaminant electron fluence was about 0.4 % and 0.8 % of the photon's fluence for 10 × 10 cm² and 40 × 40 cm² fields, respectively. Essnaahari *et al.* (2007) studied such contaminating electrons for dedicated Stereotactic radiosurgery unit, capable of generating circular radiation fields using cerroband cones with diameters of 1-5 cm at isocentre. They reported that the counts per incident electron on the target for photons of 6 MV were about 1000 times more than those of contaminant

electrons [24].

However, as shown in figure 10, these relatively small fluences of contaminant electrons contributes to 11 % and 38.8 % of the maximum dose at the surface for 10 × 10 cm^2 and 40 × 40 cm^2 fields, respectively.

As can be seen in figures 4 and 5 the fluence and mean energy from contaminant electrons, unlike those from photons, do not reduce sharply at off-axis distances outside the treatment field. The higher mean energy for contaminant electrons and the slower decrease of their fluence (lack of the fall off for the mean energy and fluence at the field border) compared to those for the photons could cause extra electron dose to the peripheral organs outside of the field size. Hence, it might be necessary to shield the critical organs even those located outside the applied field to protect these organs from such unwanted doses.

Comparing the surface dose profiles components (figures 6a and b) showed that the flatness of total dose profile inside the field was due to the electron dose (it is more pronounced for the field size of 40 × 40 cm^2).

Considering the photon beam used here, 18 MV, we assumed conveniently that the calculated surface doses could be attributed entirely from air-contaminating electrons. The dose contribution from phantom-generated electrons at the surface had negligible value which was true if all the secondary electrons had moved in the forward direction [25]. On the other hand, Nilsson and Brahme (1985) reported that the backscattered photons may produce electrons toward the surface or the produced forward electrons may be scattered backward that would increase the surface dose (3 % for ^{60}Co γ-rays and 1 % for 21 MV X-rays) [26].

The air-generated electrons dose (at surface dose) was 3.5 % and 7 % for SSD of 100 and 120 cm, figure 8a and b, respectively. Our data about the air and head components of electron dose were consistent with the others. The results of Sjorgen and Karlsson (1996) showed 4-5 times larger values for the contribution of head than the contribution of air for 20 MV at SSD of 100-120 cm [10]. As a result, the majority of contaminant electrons were produced from the accelerator head. The air-generated contaminant electrons (the air gap between Linac's head and phantom surface) were also significant and they increased with the SSD.

An increasing electron contamination was observed with field size (figure 9). Such result was expected since more opening of the collimators (larger field sizes) caused more electrons out from the head. Furthermore, for each field size, the contaminant dose decreased with depth. This contaminant dose saturated at smaller field for deeper depths. Malataras *et al.* (2001) reported the flattering filter to have the main contribution to produce contaminant electrons in Linacs [7] which had confirmed these saturated values. Studies on electron contamination sources in linacs have shown that for wide opening of the collimators, the main sources showed FF and the air below it [7]. Mesbahi *et al.* (2007) reported that the absolute electron fluence per incident electron for whole energy range showed 4% higher fluence for Elekta linac compare to Varian linac for 6 MV photons [2]. They discussed that the FF absorbs the secondary electrons generated in the target, primary collimator and the air inside the head. The secondary electrons generated by the FF produced a wide energy spectrum with mean energies of the same order of the bremsstrahlung spectrum. In another study, Mesbahi *et al.* (2009) reported that removing flattening filter would increase contamination electron fluence (normalized to photon fluence) up to 1.6 times, which has caused more skin dose for patients [27].

Our Monte Carlo calculated data about the contaminating electron dose, from 6.1 % for 5 × 5 cm^2 to 38.8 % for 40 × 40 cm^2, were within the other's data as followed. One can find some differences between our data and others, due to different field sizes, SSDs, energies, models of linacs and so on.

Hounsell and Wilkinson (1999) reported that contaminating electrons caused an increase of 25 % of the surface dose relative to the depth of the maximum dose [28]. For 6, 10 and 24 MV photon beams (varian Linac, 10 × 10 cm^2), Jursinic and Mackie (1996) showed electron contaminants to be responsible about 3%, 5% and 12% of the surface dose relative to the maximum dose, respectively [29]. An increase of 22 % of the surface dose relative to the dose at 7 cm depth (10 MV, 30 × 30 cm^2 and SSD = 100 cm) reported by Sixel and Podgorsak (1994) [30]. Zhu and Palta (1998) reported that the maximum surface dose from contaminating electrons varied from 1% to 33% for 8 MV and 2% to 44% for 18 MV in range of field sizes from 5 × 5 cm^2 to 40 × 40 cm^2 at SSD =100 cm [9]. Their results also indicated an increase of 1% for 8 MV and 2.3% for 18 MV at a depth of maximum dose. Recently, Ding (2002 b) studied the contribution of charged particles at the surface doses by Monte Carlo method [23]. His results for 6 MV showed that the maximum surface doses from charge particles were 7% for a 10 × 10 cm^2 field and 21% for a 40 × 40 cm^2 field. At 18 MV, the corresponding doses were up to 11% and 29%. However, the fluence of these incident charged particles was less than 1% of incident photon fluence in all cases. For 18 MV, the contributions of these charged particles were 4% and 6% even at depth of maximum dose (=3 cm) for 10 × 10 cm^2 and 40 × 40 cm^2 fields, respectively. A Monte Carlo approach by Malatara *et al.* (2001) showed that the contribution of the secondary contamination electrons on the surface dose (Saturne-25 and -41, SSD = 100 cm and wide opening jaws) was 16 % for 6 MV and 12 MV, 6 % for 15 MV and 17 % for 23 MV [7]. The increase of the dose at maximum dose depth was about 2 % for energies of 6, 12 and 15 MV and 4 % for the 23 MV. The contributions of the electron contamination to the central-axis depth-dose were calculated and at the surface (normalized to the depth of 10 cm) constituted between 6 % of maximum dose for the 4 MV beam and 11 % of maximum dose for the 25 MV beam.

A deviation from exponential decrease with depth (figure 9) can be seen from calculated absorbed doe curves. Bjamgard *et al.* (1995), Sjogren *et al.* (1996) and Zhu and Palta (1998) also reported this change in the shape of curves in the surface region [9, 10, 22]. Furthermore, the discrepancies of about 5% have been observed by Ding (2002) in the buildup region for the field with the lead foil between calculated dose with Monte Carlo method and measurement method [31]. Abdel -Rahman *et al.* (2005) and Vassiliev *et al.* (2006) reported that for smaller depths and small field sizes Monte Carlo simulations over estimated the dose in the buildup region while for larger field sizes Monte Carlo simulations underestimated the dose in the buildup region [32, 33]. Hartmann Siantar *et al.* (2001) suggested that this discrepancy was caused by a source of electrons in the Linac head that was not considered for Monte Carlo simulation of the head [34]. On the other hand, a study by Ding showed that this electron contaminant was not due to this discrepancy [31]. The amount of neutron dose in a high energy photon beam reported by Nath *et al.* (1993) was too small to explain the discrepancies [35]. Further studies are needed to find the true cause of this discrepancy of absorbed doses at the buildup region between Monte Carlo calculation and measurement.

The electron contamination dose was independent of the SSD in the range of 100 cm to 120 cm, but it showed slight dependence on the lower or the larger SSDs (figure 10). These results were consistent with the results from Zhu and Palta (1998) that reported no SSD dependence for 8 MV in range of 90 to 140 cm and for 18 MV at range of 90-120 cm [9]. Furthermore, their result showed a decrease for 18 MV at SSD = 140 cm. This independent also reported by Sjogren and Karlsson (1996) for 20 MV on different two Linacs at SSD of 80, 100, and 120 cm [10]. The increased dose at smaller SSDs (for example at SSD = 90 cm) and

decreased dose at SSDs (SSD = 140 cm) may be explained by this reason that the head generated electrons had a width angular distribution and spread out more at larger SSDs, Therefore, head-generated electrons had more contribution at shorter SSDs compared to larger SSDs. Furthermore, to achieve a certain field size at a shorter SSD, more opening of jaws was needed (7 cm for SSD = 90 cm compared to SSD = 140 cm in the case of 40 × 40 cm^2) that increase the amount of the head generated electrons spread out from the head. Nevertheless, different results for electron dose dependence to SSD reported by authors. Some results showed no dependence of electron contaminant dose with SSD [9, 10, 20, 28, 36], conversely, others indicated a decrease [9, 37-39]. According to these studies, electron contaminant dose variations could be caused by dependence of the electron sources (air and Linac head) to the SSD, field size, and energy. The air-generated electrons were less energetic than the Linac head electrons because the atomic numbers of air were lower than those in treatment-head materials. Therefore, air-generated electrons contribution at depth dose decreases with depth compared to head-generated electrons contribution. Furthermore, according to our results, the SSD interval selection and its range had some effect on electron contaminant dose.

Locating a shadow tray inside the beam direction increased the contaminant electron dose from 2.3 % for 10 × 10 cm^2 up to 21.4 % for 40 × 40 cm^2 field size compare to fields without tray (see figure 11). Clearly, the tray stoped low energy electrons from the upstream components, air and Linac head structures. Conversely, attenuating tray made of aluminum with low atomic number, ^{13}Al, became a source of the contaminating Compton electrons causing these increases. The increase of electron contaminant with the tray reported by other authors [9, 10, 26]. Lopez Medina *et al.* (2005) reported that if a tray is used as beam modifier, electron contamination would increase. But the energy of these electrons would be similar to that of electrons coming from the treatment head [3]. Figure 11 also represented analytically fitted curves. In addition to the reasons mentioned previously for the differences between calculated and analytical curves, it should be mentioned that our 0.6 cm thick tray made of aluminum located at 34.6 cm from surface of phantom while the extracted fitting data from Zhu and Palta (1998) study [9] belonged to an acrylic tray located at 33 cm (0.64 cm thick). This deviation also was seen by Lopez Medina *et al.* (2005), especially for smaller field sizes with air-generated electrons which must have been considered independently; because, they had different energetic spectrum and dosimetric influence [3].

The contaminant electron dose increased further (3.5 % for 10 × 10 cm^2 and 4.4 % for 20 × 20 cm^2, see figure 12) when a shaping block was located upper on the shadow tray compared to the field with tray only. However, the located block on a tray would block some of the introduced electrons from upstream components (flattering filter, beam monitor chamber, upper air column and collimators) and cover some parts of the tray surface which would reduce the electron reached to surface of phantom, but penetrating the block-produced electrons would increase the electron contamination depth dose. Therefore, the contaminating electrons from shaping block would be considerable when the shadow tray was removed from the beam direction and had a large dependence on the energy and distance to the surface [10, 40]. The magnitudes of additional increases for field size of 20 × 20 cm^2 are consistent with values published by Zhu and Palta (1998) [9]. For field size of 10 × 10 cm^2 our surface doses from contaminating electrons, 18 % form calculation and 21 % from analytical fitting, are in good agreement with reported values of Sjogren and Karisson (1996) for 20 MV photon beam, 17 % from measurement and 21% from fitting study [10]. Ostinell *et al.* (2000) reported that this

secondary electron contamination of the photon beam upon the calibration factor of the diode in the case of tray alone, or with tray and blocks was stronger than in the open field [41].

When a steel wedge was located into the beam direction the contaminant electron dose decreased compared to the standard field. This was expected since the wedge stopped the most electrons coming from upstream head and air components [13, 20]. Conversely, some electrons were produced in the wedge, but the amount of these contaminating electrons was smaller than the coming electrons from the upstream components, especially from the beam monitor chamber and flattening filter, or form shadow tray and shaping block. Furthermore, the produced electrons from the steel wedge might have larger scattering angle and located at far distance (43.4 cm) from the surface of phantom compared to tray (34.6 cm). Momennezhad *et al.* (2010) reported that as the wedge angle increased (from 15° up to 60°), the electron contamination of photon beam decreased. This decrease indicated that the number of electrons produced in the wedge was less than the number of electrons eliminated by the wedges. The increase of electron/photon ratio with increase of wedge angle indicates that the photon fluencies decreased more with wedges compared to electron fluencies [13].

This information enhanced the knowledge about the clinical photon beams and the associated contaminant electrons with them. These results could be important when used in TPSs in clinical dosimetry especially in the cases of additional accessories such as the external wedge, the shadow tray, and the shaping block. It also demonstrated the accuracy of the Monte Carlo technique in simulating the contaminant electrons of therapeutically photon beams. In the future work that is in progress, the effect of removing flattening filter from Linac's head on dosimetric properties of photon and contaminating electrons would be studied.

ACKNOWLEDGMENT

This study was supported financially by research affaires of Tehran University of Medical Sciences, Tehran, Iran.

REFERENCES

1. Parsai EI, Shvydka D, Pearson D, Gopalakrishnan M, Feldmeier JJ (2008) Surface and build-up region dose analysis for clinical radiotherapy photon beams. *Applied Radiation and Isotopes,* ***10:*** *438-1442.*
2. Mesbahi A, Mehnati P, Keshtkar A (2007) A comparative Monte Carlo study on 6MV photon beam characteristics of Varian 21EX and Elekta SL-25 linacs. *Iran J Radiat Res,* ***5:*** *23-30.*
3. Lopez Medina A, Teijeiro A, Garcia J, Esperon J, Terron JA, Ruiz DP, Carrion MC (2005) Characterization of electron contamination in megavoltage photon beams. *Med Phys*, ***32:*** *1281-1292.*
4. Lopez Medina A, Teijeiro A, Salvador F, Medal D, Vazquez J, Salgado M, Carrion MC (2004) Comparison between TG-51 and TRS-398: electron contamination effect on photon beam-quality specification. *Phys Med Biol*, ***49:*** *17-32.*
5. Harper NR, Metcalfe PE, Hoban PW, Round WH (1991) Electron contamination in 4 MV and 10 MV radiotherapy X-ray beams. *Australas Phys Eng Sci Med* ***14:*** *141-145.*
6. Klevenhagen SC (1991) Determination of absorbed dose in high-energy electron and photon radiation by means of an uncalibrated ionization chamber. *Phys Med Biol*, ***36:*** *239-253.*
7. Malataras G, Kappas C, Lovelock DM (2001) A Monte Carlo approach to electron contamination sources in the Saturne-25 and -41. *Phys Med Biol*, ***46:*** *2435-2446.*
8. Damrongkijudom N, Oborn B, Butson M, Rosenfeld A (2006) Measurement of magnetic fields produced by a "magnetic deflector" for the removal of electron contamination in radiotherapy. *Australas Phys Eng Sci Med*, ***29:*** *321-327.*
9. Zhu TC and Palta JR (1998) Electron contamination in 8 and 18 MV photon beams. *Med Phys*, ***25:*** *12-19.*
10. Sjogren R and Karlsson M (1996) Electron contamination in clinical high energy photon beams. *Med Phys*, ***23:*** *1873-1881.*
11. Parthasaradhi K, Prasad SG, Rao BM, Lee Y, Ruparel R, Garces R (1989) Investigation on the reduction of electron contamination with a 6-MV X-ray beam. *Med Phys*, ***16:*** *123-125.*
12. Rogers DW (1999) Correcting for electron contamination at dose maximum in photon beams. *Med. Phys*, ***26:*** *533–537.*
13. Momennezhad M, Bahreyni Toosi M.T, Sadeghi R, Gholamhoseinian H, Nasseri Sh (2010) A Monte Carlo simulation and dosimetric verification of physical wedges used in radiation therapy. *Iran J Radiat Res*, ***7:*** *223-227.*
14. Yadav G, Yadav RS, Kumar A (2009) Skin dose estimation for various beam modifiers and source-to-surface

distances for 6MV photons. *J Med Phys*, **2:** *87-92.*
15. Pasquino M, Borca VC, Tofani S, Ozzello F (2009) Verification of Varian enhanced dynamic wedge implementation in MasterPlan treatment planning system. *Journal of Applied clinical Medical Physics*, **2:** *11-20.*
16. Starkschall G, Steadham RE, Jr., Popple RA, Ahmad S, Rosen II (2000) Beam-commissioning methodology for a three-dimensional convolution/superposition photon dose algorithm. *J Appl Clin Med Phys*, **1:** *8-27.*
17. Cozzi L, Buffa FM, Fogliata A (2001) Dosimetric features of linac head and phantom scattered radiation outside the clinical photon beam: experimental measurements and comparison with treatment planning system calculations. *Radiother Oncol*, **58:** *193-200.*
18. Almond PR, Biggs PJ, Coursey BM, Hanson WF, Huq MS, Nath R, Rogers DW (1999) AAPM's TG-51 protocol for clinical reference dosimetry of high-energy photon and electron beams. *Med Phys*, **26:** *1847-1870.*
19. Walter LS (2002) LANL (Los Alamos National Laboratory) Monte Carlo N-Particle transport code system for multiparticle and high energy applications version 2.4.0, Ref Type: Serial (Book, Monograph)
20. Beauvais H, Bridier A, Dutreix A (1993) Characteristics of contamination electrons in high energy photon beams. *Radiother Oncol*, **29:** *308-316.*
21. Ahnesjo A and Andreo P (1989) Determination of effective bremsstrahlung spectra and electron contamination for photon dose calculations. *Phys Med Biol*, **34:** *1451-1464.*
22. Bjarngard BE, Vadash P, Zhu T (1995) Doses near the surface in high-energy X-ray beams. *Med Phys*, **22:** *465-468.*
23. Ding GX (2002) Energy spectra, angular spread, fluence profiles and dose distributions of 6 and 18 MV photon beams: results of monte carlo simulations for a varian 2100EX accelerator. *Phys Med Biol*, **47:** *1025-1046.*
24. Esnaashari KN, Allahverdi M, Gharaati H, Shahriari M (2007) Comparison of measured and Monte Carlo calculated dose distributions from circular collimators for radiosurgical beams. *Iran J Radiat Res,* **5:** *31-36.*
25. Mackie TR, Scrimger JW (1982) Contamination of a 15-MV photon beam by electrons and scattered photons. *Radiology*, **144:** *403-409.*
26. Nilsson B (1985) Electron contamination from different materials in high energy photon beams. *Phys Med Biol*, **30:** *139-151.*
27. Mesbahi A (2009) A Monte Carlo studies on neutron and electron contamination of an unflattened 18-MV photon beam. *Applied Radiation and Isotopes*, **67:** *55-60.*
28. Hounsell AR and Wilkinson JM (1999) Electron contamination and build-up doses in conformal radiotherapy fields. *Phys Med Biol*, **44:** *43-55.*
29. Jursinic PA and Mackie TR (1996) Characteristics of secondary electrons produced by 6, 10 and 24 MV X-ray beams. *Phys Med Biol*, **41:** *1499-1509.*
30. Sixel KE and Podgorsak EB (1994) Buildup region and depth of dose maximum of megavoltage X-ray beams. *Med Phys*, **21:** *411-416.*
31. Ding GX (2002) Dose discrepancies between Monte Carlo calculations and measurements in the buildup region for a high-energy photon beam. *Med Phys*, **29:** *2459-2463.*
32. Vassiliev ON, Titt U, Kry SF, Ponisch F, Gillin MT, Mohan R (2006) Monte Carlo study of photon fields from a flattening filter-free clinical accelerator. *Med Phys*, **33:** *820-827.*
33. Abdel-Rahman W, Seuntjens JP, Verhaegen F, Deblois F, Podgorsak EB (2005) Validation of Monte Carlo calculated surface doses for megavoltage photon beams. *Med Phys*, **32:** *286-298.*
34. Hartmann Siantar CL, Walling RS, Daly TP, Faddegon B, Albright N, Bergstrom P, Bielajew AF, Chuang C, Garrett D, House RK *et al.* (2001) Description and dosimetric verification of the PEREGRINE Monte Carlo dose calculation system for photon beams incident on a water phantom. *Med Phys*, **28:** *1322-1337.*
35. Nath R, Meigooni AS, King CR, Smolen S, d'Errico F (1993) Superheated drop detector for determination of neutron dose equivalent to patients undergoing high-energy X-ray and electron radiotherapy. *Med Phys*, **20:** *781-787.*
36. Purdy JA (1986) Buildup/surface dose and exit dose measurements for a 6-MV linear accelerator. *Med Phys*, **13:** *259-262.*
37. Klein EE and Purdy JA (1993) Entrance and exit dose regions for a Clinac-2100C. *Int J Radiat Oncol Biol Phys*, **27:** *429-435.*
38. Kim S, Liu CR, Zhu TC, Palta JR (1998) Photon beam skin dose analyses for different clinical setups. *Med Phys*, **25:** *860-866.*
39. Rao BM, Prasad SG, Parthasaradhi K, Lee Y, Ruparel R, Garces R (1988) Investigations on the near surface dose for three 10-MV X-ray beam accelerators with emphasis on the reduction of electron contamination. *Med Phys*, **15:** *246-249.*
40. Nilsson B and Brahme A (1986) Electron contamination from photon beam collimators. *Radiother Oncol*, **5:** *235-244.*
41 Ostinelli A, Gelosa S, Cacciatori M, Frigerio M, Monti A, Tognoli P (2000) The effects of focus-skin distance and shaping block tray on the calibration factor of in-vivo dosimetry diodes. *Strahlenther Onkol*, **176:** *528-531.*